The Iranian Journal of Mechanical Engineering Transactions of ISME
Journal homepage: https://jmee.isme.ir/
Vol. 25, No. 2, 2024, pp. 78-92

Research Paper

DOI: https://doi.org/10.30506/jmee.2024.2039375.1357

Analysis of an Efficient Circular Solar Air Heater

Mohammad Omidpanah[*]
Assistant Professor

Seyed Abdolreza Gandjalikhan Nassab[†]
Professor

The main contribution of this study is to present a circular solar air heater with two air passes for higher performance compared to conventional plane solar collectors. The flow of inlet cold air in a radial direction leads to an effective convective heat transfer with a thin boundary layer over a large surface area. Also, due to the shape of the solar collector, it occupies less space than the rectangular types. For simulation via the COMSOL Multi-physic software, the 2-D asymmetric turbulent airflow equations are solved by the finite element method using the turbulence model and the conduction equation is employed for temperature computations inside the solid elements. From the obtained results, up to 85% thermal efficiency is seen for the deigned collector at 0.06 kg/s air mass flow rate. The obtained efficiency shows about 100% improvement compared with the performance of the smooth duct conventional solar air heater. The numerical findings can be considered as a good reference to find an alternative for efficient solar collectors.

Keywords: Circular solar air heater, Asymmetric, Efficiency, CFD

1 Introduction

Solar energy as a wide inexpensive renewable and clean energy source can be considered a good alternative in the consumption of energy. The solar air heaters are well-known collectors in converting solar incoming radiation into air enthalpy as a useful heat energy. Among them, the plane solar air heaters (SAHs) shown in Fig. (1) have a simple structure and design with low maintenance, but they are inefficient due to low air conductivity and heat capacity.
To enhance the rate of convection heat transfer, many investigators seek different techniques which can be listed with the following main subjects:
a) Enhancing the incoming solar irradiation [1, 2].

[*]Corresponding author, Assistant Professor, Department of Mechanical Engineering, National University of Skills (NUS), Tehran, Iran, Momidpanah@nus.ac.ir
[†]Professor, Mechanical Engineering Department, School of Engineering, Shahid Bahonar University of Kerman, Kerman, Iran, ganj110@uk.ac.ir

Received: 2024/08/22, Revised: 2024/11/27, Accepted: 2024/12/08

b) Reduction of thermal losses [3, 4].
c) Increasing the convection coefficient [5, 6].
d) Extension of surface area [7, 8, 9].
e) Using phase change materials (PCM) [10, 11].
f) Employing porous medium [12, 13].
g) Use of jet impingement [14, 15].

In (2022), a theoretical and experimental study about using porous medium in the construction of SAHs was done by Singh [16]. The importance of that work is due to the obtained highest efficiency increase of solar collectors by the applied method. The suggested SAH with the serpentine porous wavy channel shown in Fig. (2) was said to have a thermal efficiency that is roughly 1.8 times greater than that of the conventional smooth duct SAHs.

An efficient and simple structure circular-shaped SAH was designed by the second author for the purpose of performance improvement [17]. A convective airflow with a vortex pattern inside the vessel of the heater took place by entering the inlet air in a tangential direction. This technique provides a long path for the airflow from the inlet to the outlet section with turbulence generation and high rate of mixing between the rotating air layers. The use of converged air duct in the SAHs for flow acceleration and convection enhancement was introduced by the second author [18]. The numerical findings in that study revealed the positive effect of the applied technique in efficiency increase.

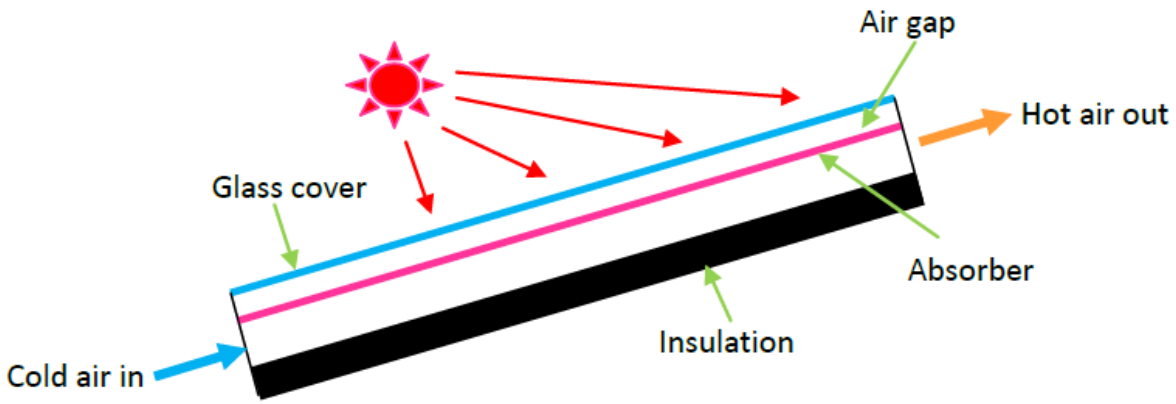

Figure 1 Schematic of a conventional plane SAH

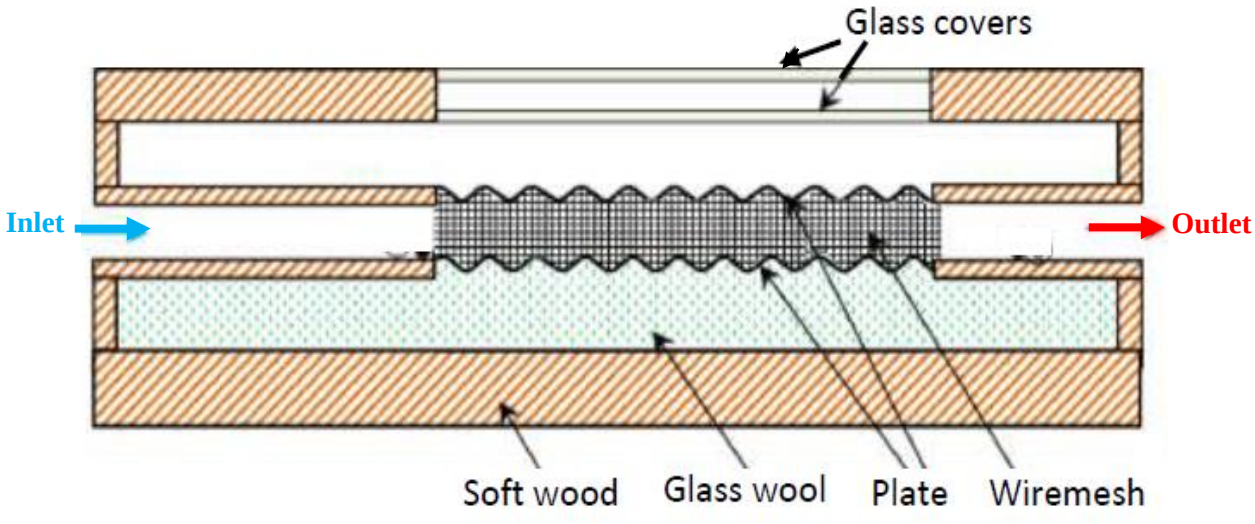

Figure 2 Geometry of the SAH with a wavy porous channel [16].

In all of the abovementioned studies on convection augmentation, the structure of solar collector becomes more complicated and with high pressure drop because the installations of equipment such as jet plates, baffles, fins, dimples, vortex generators, and various absorber shapes. It should be mentioned that the efficiency gain over standard plane SAHs is approximately 180% as reported in literature, despite the high costs of solar collectors with more pressure drops. This fact motivates the authors to design an effective, low-complication SAH with a simple geometry and with a high rate of convection heat transfer between the flowing air and the heated surface. As seen in Fig. (3), the cold air enters from the two inlet sections in the radial direction, such that both upper and lower surfaces of the absorber plate are in contact with the following air and an effective convection heat transfer takes place in the collector. Regarding the fact that the convection coefficient decreases along the flow direction, the main contribution of the deigned collector is the occurrence of radial convection flow with a thin thermal boundary layer started from the inlet section over a large area of circular absorber surface. So, the current study introduces a numerical simulation of the proposed SAH by simultaneous solution of the conservation of mass, momentum and energy equations at steady, two-dimensional, and asymmetry conditions, while the surface radiation is also considered into account. Finally, the performance of the designed SAH operating under different steady conditions is examined.

2 Introduction

The geometry of the simulated circular SAH is depicted in Fig. (3). It includes the glass cover, air channels, absorber, bottom plate and insulation layer.
The glass cover has a radius of R=0.5 m and the air enters into the heater in the radial direction from both above and below the absorber plate, and the hot air exits by a duct embedded in the insulation layer with $R_{out} = 4\ cm$. The bottom plate and absorber have the same geometrical and physical properties. In Table (1), the values of some geometrical parameters of the simulated SAH are reported.

Table 1 Parameter values of the test cases

Parameter	Value
Thickness of glass coverv	4 mm
Glass emissivity	0.9
Glass absorptivity	0.03
Glass transmissivity	0.95
Conduction coefficient of glass	0.8 W/mK
Conduction coefficient of insulation	0.04 W/mK
Height of air duct	1-5 cm
Thickness of absorber	4 mm
Emissivity of absorber	0.95
Conduction coefficient of absorber	400 W/mK
Inlet temperature	20 ^{o}C
Insulation thickness	4 cm
Air mass flow rate	0.01 – 0.06 kg/s

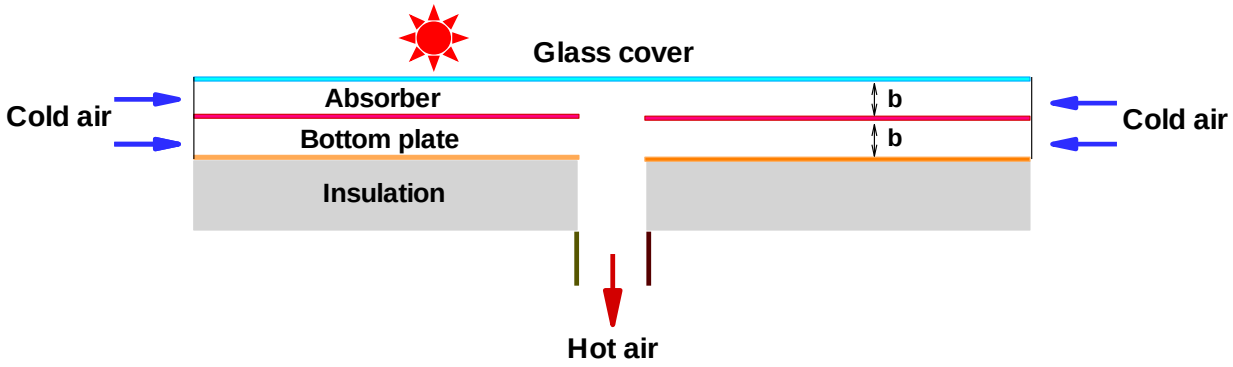

Figure 3 A schematic of the proposed SAH

The airflow enters from the inlet section due to the air blower suction, and the forced convection heat transfer occurs with the heated absorber and bottom plate surfaces. Different air mass flow rates in the range of $\dot{m} = 0.02\ kg/s$ to 0.06 kg/s are considered in several test cases. The surfaces of the insulation layer and glass cover adjacent to the surrounding are in heat transfer by convection and surface radiation with the ambient. Due to high velocity and high Reynolds number flow in the outlet duct embedded inside the insulation, the airflow becomes turbulent, such the maximum and minimum values of Reynolds number ($2\dot{m}/\pi R_{out}\mu$) for the studied test cases are 54000 and 18000, respectively, denote the turbulent regime. The preliminary simulation showed that the thermal behavior of solar collectors is much affected by the height of air ducts, b, and a great effort was made to examine the effect of this parameter by considering five values including b=1 cm to 5 cm during several test cases.

2.1 Governing equations and boundary conditions

The model is steady two dimensional, incompressible, and turbulent and the Reynolds Average Navier Stokes (RANS) equations are employed in the fluid flow computations. The k-ε model given by Patankar [19] is used in flow computation and the enhanced wall function is considered for the grid point near the solid walls. The following governing equations written in tensor forms are considered in this study:

$$\frac{\partial u_i}{\partial x_i} = 0 \tag{1}$$

$$u_j \frac{\partial u_i}{\partial x_j} = \frac{1}{\rho}\frac{\partial p}{\partial x_i} + \frac{1}{\rho}\frac{\partial}{\partial x_j}[(\mu + \mu_t)(\frac{\partial u_i}{\partial x_j} + \frac{\partial u_i}{\partial x_j})] \tag{2}$$

$$u_j \frac{\partial T}{\partial x_j} = \frac{\partial}{\partial x_j}[(\frac{\mu}{\mathrm{Pr}} + \frac{\mu_t}{\mathrm{Pr}_t})]\frac{\partial T}{\partial x_j} \tag{3}$$

Since the RNG k-ε model is employed in simulation, the turbulent kinetic energy and its dissipation rate must be computed. The equations govern to these dependent variables are:

$$\rho u_i \frac{\partial \kappa}{\partial x_i} = \frac{\partial}{\partial x_j}[(\mu + \frac{\mu_t}{\sigma_k})\frac{\partial \kappa}{\partial x_j}] + G_\kappa - \rho\varepsilon \tag{4}$$

$$\rho u_i \frac{\partial \varepsilon}{\partial x_i} = \frac{\partial}{\partial x_j}[(\mu + \frac{\mu_t}{\sigma_\varepsilon})\frac{\partial \varepsilon}{\partial x_j}] + C_{\varepsilon 1}\frac{\varepsilon}{\kappa}G_\kappa - C_{\varepsilon 2}\rho\frac{\varepsilon^2}{\kappa} \quad (5)$$

Where, the values of model constants are $C_{\varepsilon 1} = 1.44, C_{\varepsilon 2} = 1.92, \sigma_k = 1$, and $\sigma_\varepsilon = 1.3$. Also, G_k represent the turbulence kinetic energy generation due to velocity gradient. More details on the computations of k and ε are given in Ref. [19].

For temperature computation in all solid elements of SAH, the Laplace equation is solved, such that the source term, $S_T = \alpha_g q_{sun}/\delta_g$ is considered in the glass conduction due to the radiative absorption by this element. In the numerical solution of the flow equations, the velocity inlet and pressure outlet boundary conditions are employed at the inlet and outlet sections, respectively. On the upper surface of absorber, the constant heat flux $\alpha_{abs} \times q_{sun} \times \tau_g (W/m^2)$ is imposed. Also, the side wall is assumed adiabatic, and on the outer surfaces, the convection boundary condition with the equivalent convection coefficient $h_{eq} = h_{conv} + h_{rad}, is$ considered as follows: [20].

$$h_{rad} = \sigma\varepsilon_g(\frac{T_g^4 - T_{sky}^4)}{T_g - T_{amb})} \quad (6)$$

$$h_{conv} = 5.7 + 3.8V_{wind} \quad (7)$$

Where the sky temperature can be calculated as:

$$T_{sky} = 0.0552\, T_{amb}^{1.5} \quad (8)$$

3 Grid independence test and validation

To get the optimum number of elements, a grid independence test was performed. In the mesh study, five different grid sizes with 2630 to 10100 elements were examined for the test case with $q_{sun} = 1000\frac{W}{m^2}, \dot{m} = 0.04\, kg/s$ and the maximum absorber temperature as the most sensitive parameter to the grid size has been evaluated and reported in Table (2). The discretized computational domain with 7210 elements is best suited for this model beyond this mesh size, the percentage of maximum temperature variation, becomes less than 1%. In Fig. (4), the discretized computational domain is depicted.

Table 2 Mesh study

No. of elements	$T_{max}(^0C)$	Error
2630	80.48	-
3680	83.30	3.5%
5150	84.55	1.5%
7210	**85.40**	**1%**
10100	85.83	0.5%

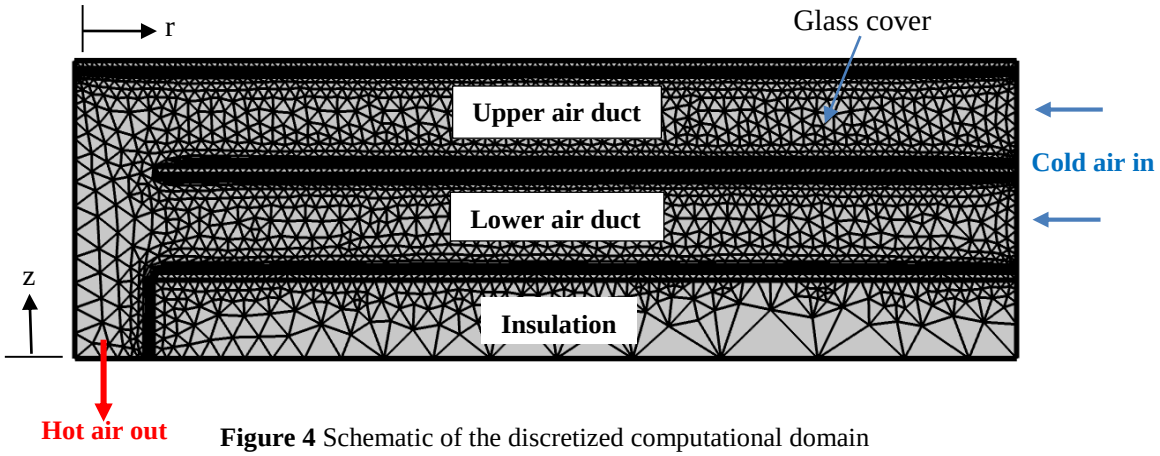

Figure 4 Schematic of the discretized computational domain

In the present simulation, the wall function is used for flow simulation adjacent to the solid walls and the minimum size of elements in the computational domain is chosen based on $y^+ \geq 30$ [21].

The applied physical model and numerical simulation were validated with the experimental data by Chabane [22]. The rectangular-shaped plane SAH, which was studied experimentally in that study, is analyzed here and the numerical results are compared with the experiment. The efficiency of SAH is evaluated at two different air mass flow rates and its distributions from 9 AM to 14 PM are plotted in Fig. (5). This figure shows the performance improvement as the mass flow rate gets higher values, such that the maximum efficiency occurs at 1 PM, while the incoming solar radiation has its maximum value. The maximum difference between the predicted thermal efficiency and experimental data with a percentage of 5.5% takes place for the air mass flow rate $\dot{m} = 0.01\ kg/s$, at 11 Am, which shows the acceptable accuracy of computations.

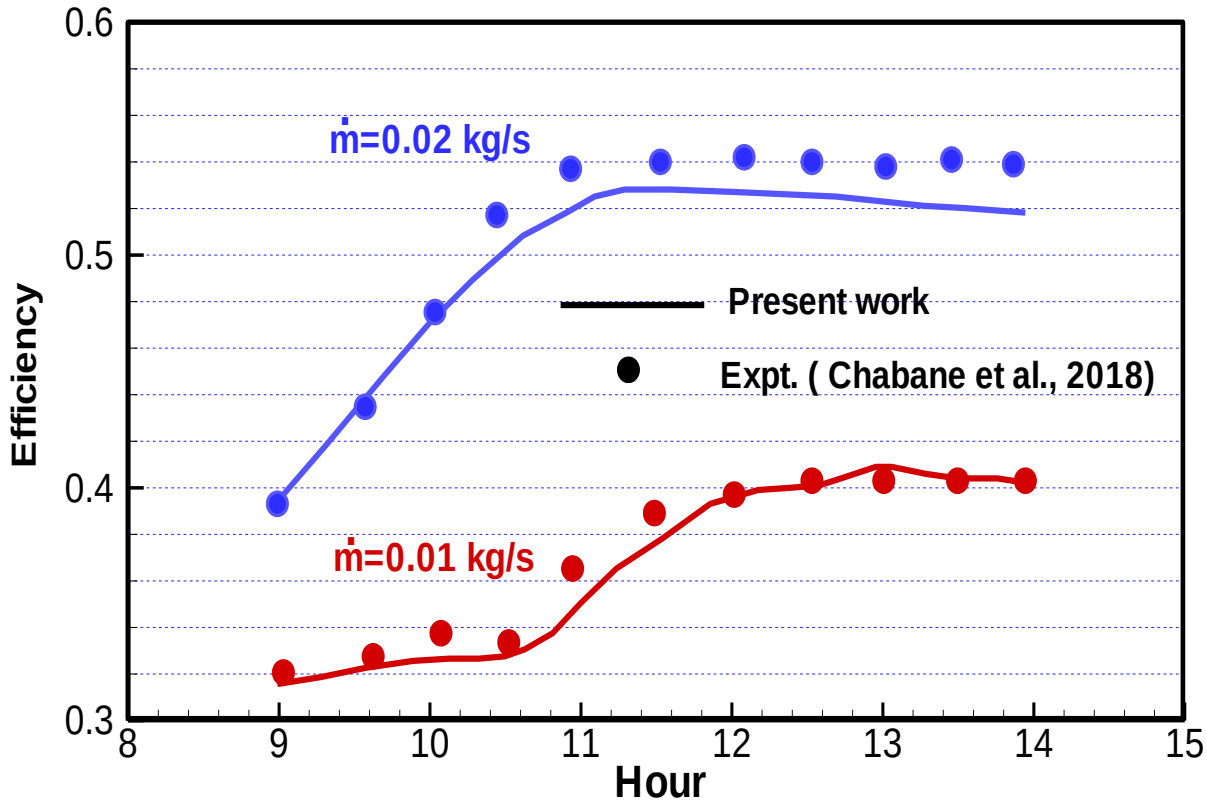

Figure 5 SAH efficiency at different hours, comparison with experimental data [22]

4 Results

The numerical results of the flow and thermal behavior of SAH operating under different steady conditions are reported in this section. As noted before, the main factor in providing the convection enhancement is the occurrence of convective flow with a thin thermal boundary layer at the upstream side along a large surface area. In several test cases analyzed in this paper, the performance of SAH was verified at different air mass flow rates and the height of air ducts under the incident sun heat flux of $q_{sun} = 1000\ W/m^2$. In Fig. (6), the contours of velocity magnitude in the upper and lower air ducts of heater are plotted. This figure shows a similar pattern for the velocity field in all test cases with a decrease in the air velocity inside the air ducts as the height b increases. As expected, a high air velocity is seen through the outlet channel due to the narrow cross-section.

To assess the effect of duct height on the thermal behavior of solar collectors, the temperature contour plots inside the whole parts of SAH are plotted in Fig. (7) at three different values of the parameter b. In all test cases, the highest temperature belongs to the absorber where the incoming solar irradiation is absorbed such that for the case with b=5 cm, the highest temperature takes place. Also, due to the surface radiation, the bottom plate and glass cover have relatively high temperatures and some of the energy conversion between solar radiation into air enthalpy takes place by convection with these elements. Comparison between the contour plots in Fig. (7) demonstrates higher performance for the designed solar collector for small values of the duct height b. It is due to the high convection coefficient between the flowing air and the heated surfaces when the air velocity gets higher values in the case of using a narrow air passage. As seen in Fig. (7), a considerable decrease in the absorber plate temperature also happens in the test cases with a smaller height of the air duct, such that the maximum absorber temperature in the case of b=1 cm is about 62 C, which is much smaller than 83 C that happens at b=5 cm. To have more clear figures about the thermal behavior of SAH and notice the asymmetry condition, the 2-D isotherm plots at different values of b are drawn in Fig. (8).

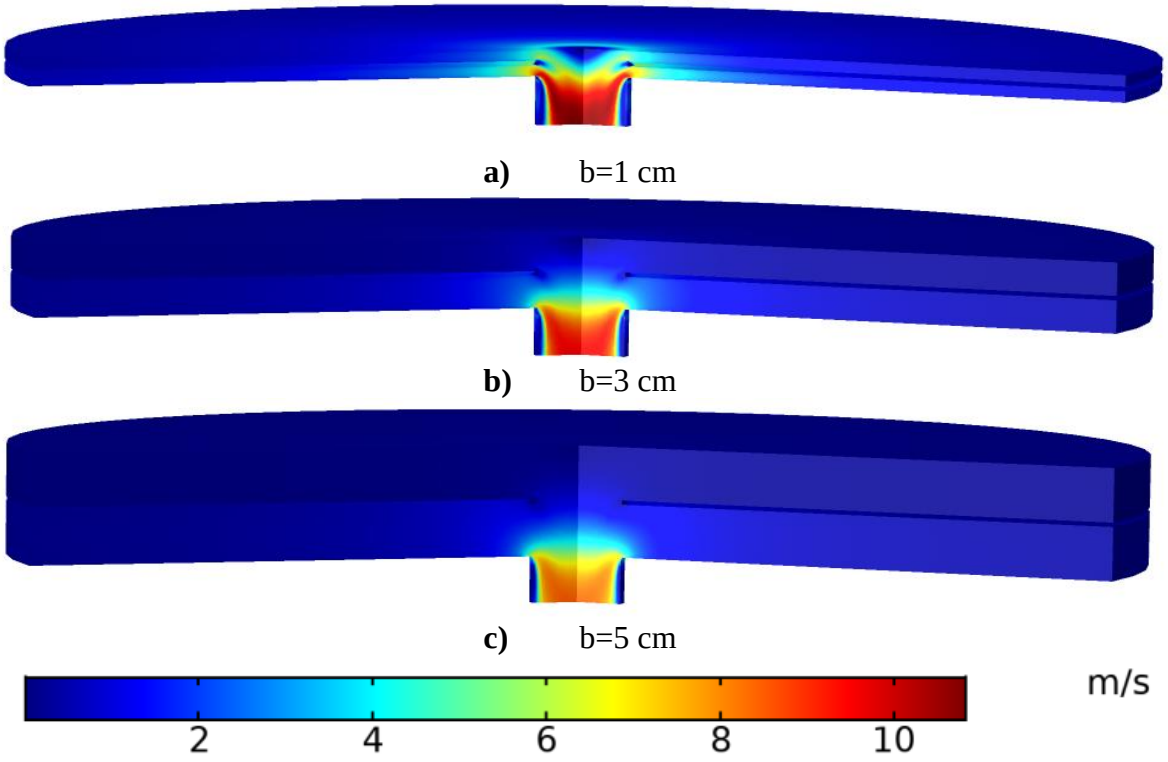

Figure 6 Velocity magnitude contours, $q_{sun} = 1000\frac{W}{m^2}, \dot{m} = 0.04\ kg/s$

As seen, the absorber temperature is much affected by the parameter b and decreases with decreasing in the value of duct height. It is due to the convection enhancement and converting more rate of radiant energy into air enthalpy in narrow air passages with higher velocity. Besides, the glass cover which is under the surface radiation with the heated absorber receives less rate of radiant energy and finally lower rate of heat loss from the thermal system leads to a higher performance for the solar collector.

In Fig. (9), the temperature variations across the SAH at different radial sections are plotted. A linear trend is seen for temperature distributions in all solid elements, while the air temperature in both upper and lower ducts has different profiles. It is seen that at each radial section r=cte, more rate of heat transfer takes place into the lower airflow which is between the two heated surfaces including the absorber and bottom plate. Comparison between the curves plotted in three different radial sections r=2R/3, R/2, and R/3 shows how the convective airflows receive thermal energy from the heated surfaces. About the temperature variation shown in Fig. (9), one can recall the very high air temperature gradient adjacent to the absorber surface which is due to the very low air thermal conductivity compared to the conduction coefficient of the absorber plate.

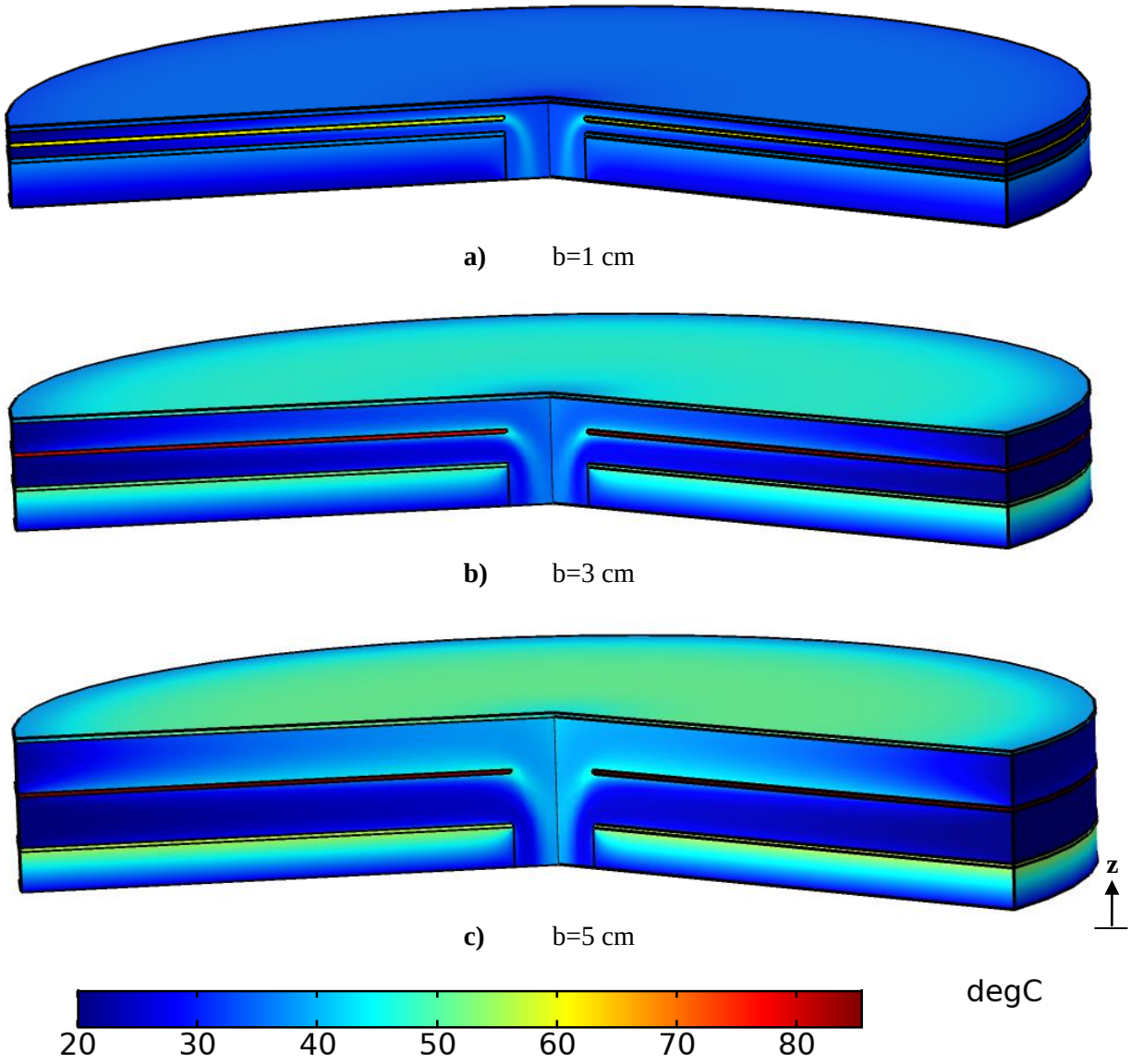

Figure 7 Temperature fields at different values of b, $q_{sun} = 1000 \frac{W}{m^2}, \dot{m} = 0.04\ kg/s$

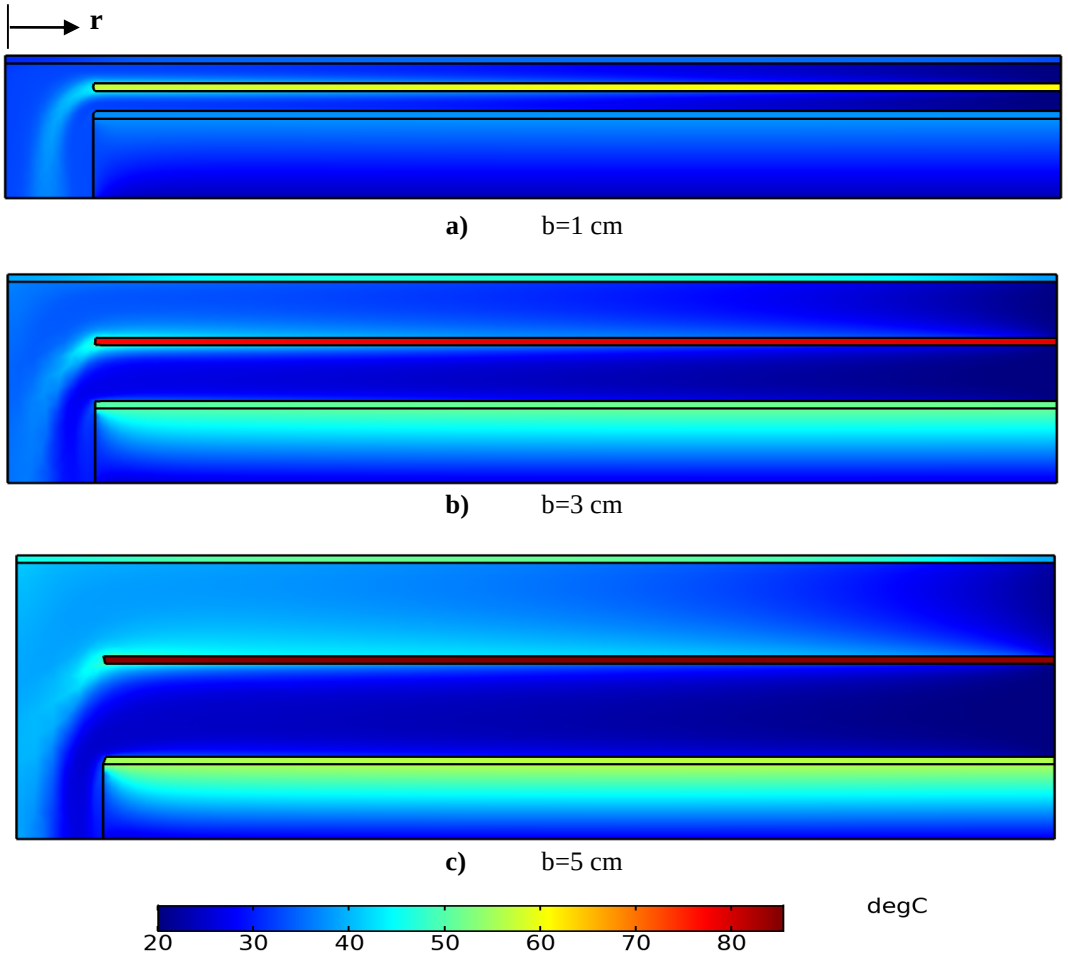

Figure 8 Two-dimensional isotherm plots at different values of b, $q_{sun} = 1000 \frac{W}{m^2}, \dot{m} = 0.04\ kg/s$

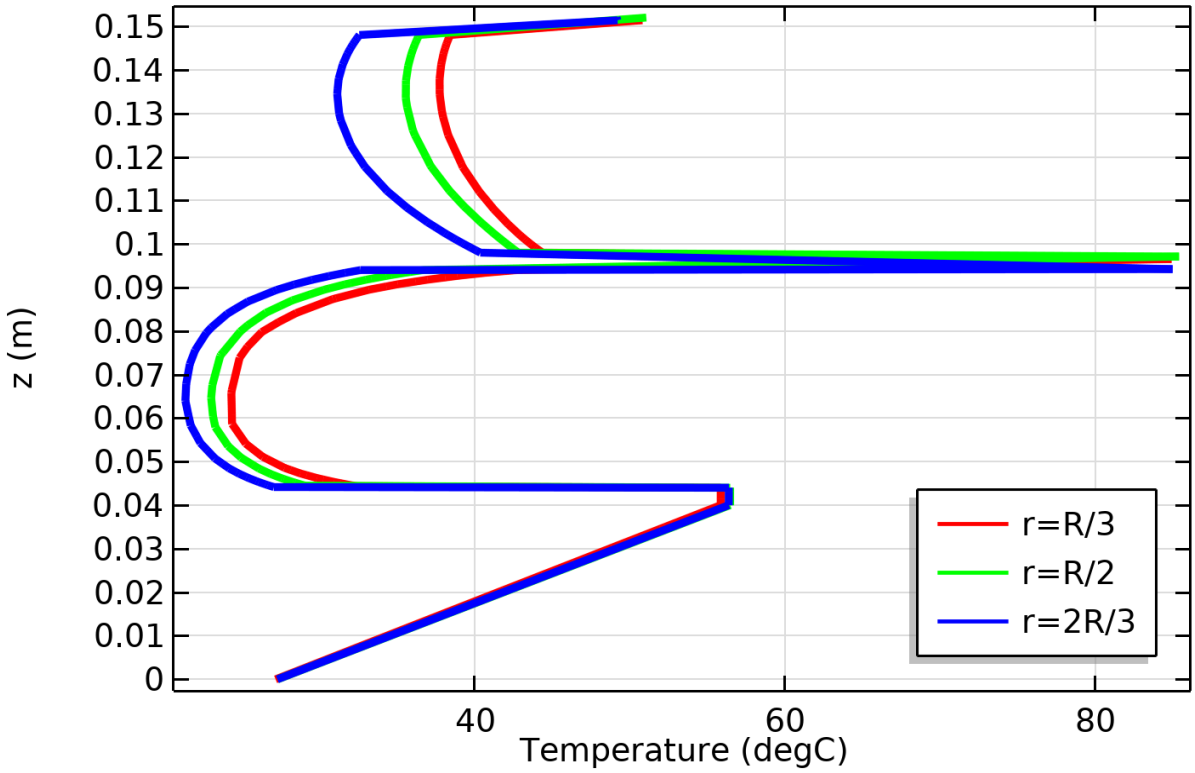

Figure 9 Temperature variation in z-direction, b=5 cm, $q_{sun} = 1000 \frac{W}{m^2}, \dot{m} = 0.04\ kg/s$

The pressure contour drawn in Fig. (10) shows a relatively high-pressure zone with almost uniform distribution inside the upper and lower ducts, while a low-pressure zone is seen at the outlet chamber. The amount of pressure drop inside the circular SAH for the cases b= 1 cm and 2 cm are 68 Pa and 32 Pa, respectively, which are higher than the pressure drop in smooth channel conventional plane SAH. This behavior is due to the difference between the flow patterns in these solar collectors.

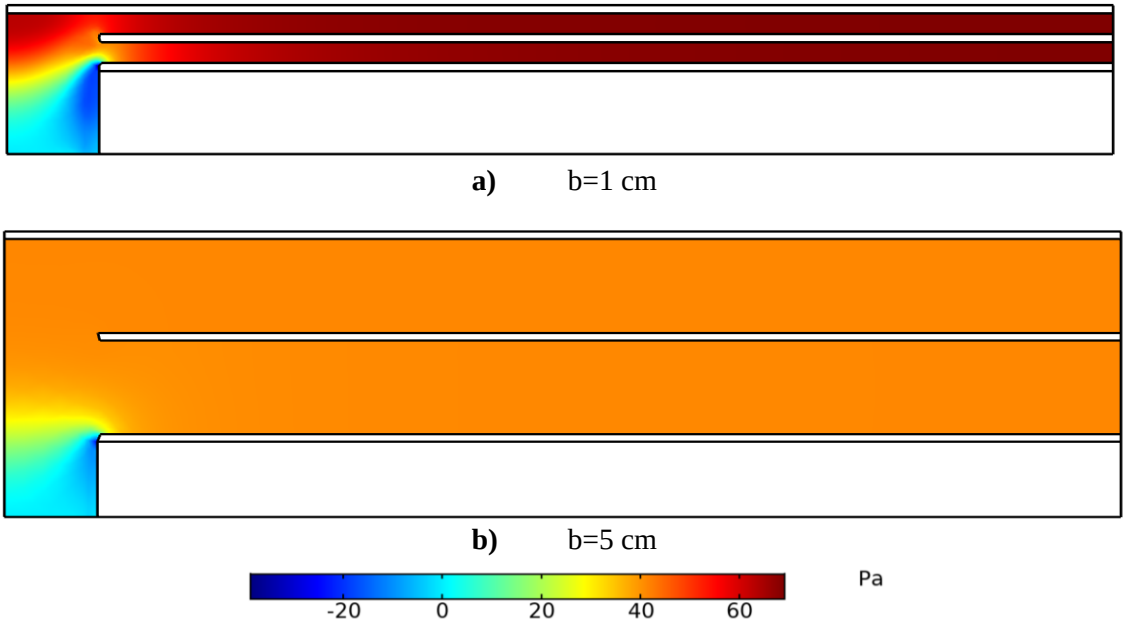

Figure 10 2-D isobar plots at different values of b, $q_{sun} = 1000 \frac{W}{m^2}, \dot{m} = 0.04\ kg/s$

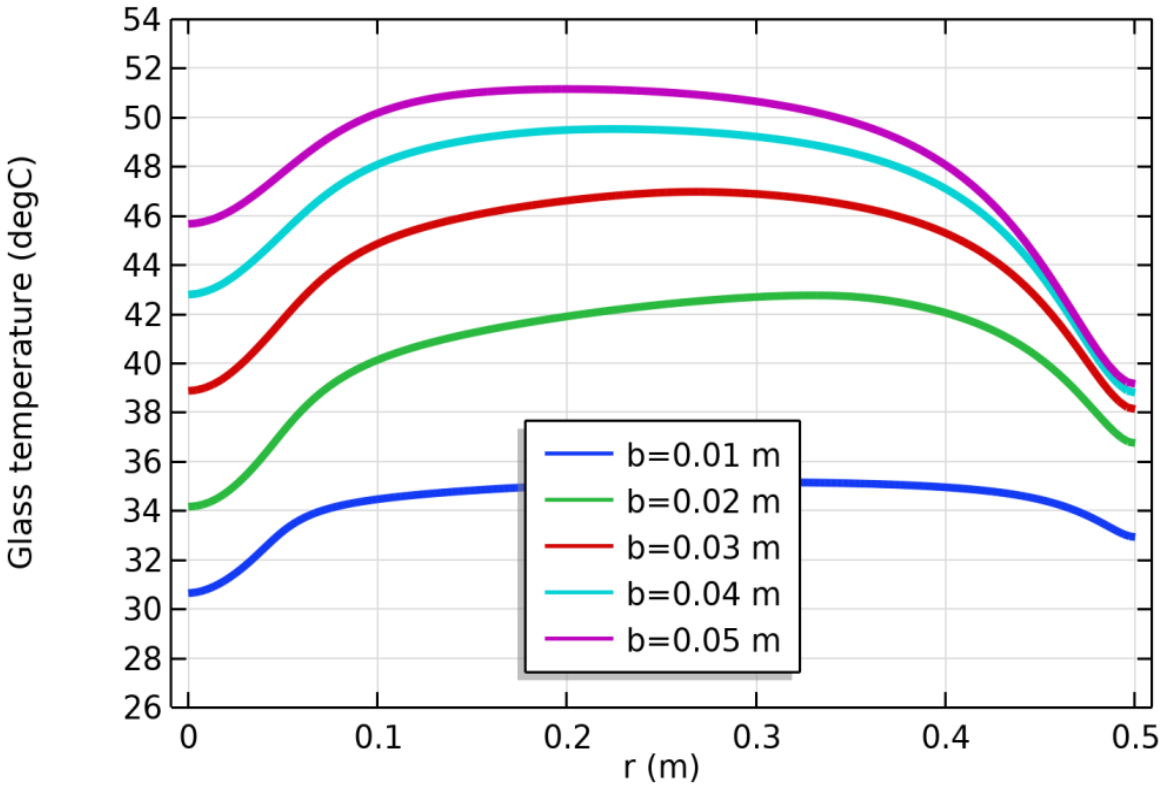

Figure 11 Glass temperature distributions in radial direction at different values of the parameter b $q_{sun} = 1000 \frac{W}{m^2}, \dot{m} = 0.04\ kg/s$

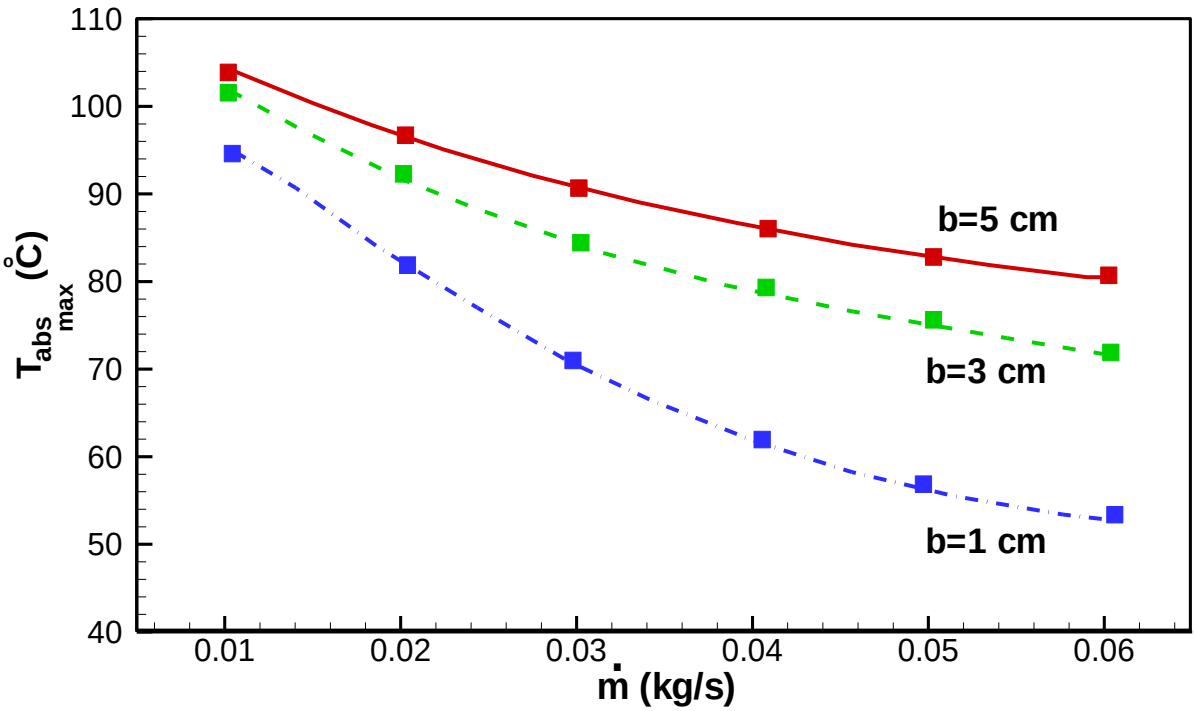

Figure 12 Maximum absorber temperature variation with air mass flow rate, $q_{sun} = 1000 \frac{W}{m^2}$

Since, the major part of heat loss form SAHs takes place via the glass cover whose temperature is relatively high due to the surface radiation with the heated absorber, the distributions of glass cover temperature along the radial direction are calculated and plotted in Fig. (11) at different values of the parameter b. As seen, the maximum glass temperature happens near the radial section r=R/2, and the local minimum temperatures at r=0 and R, because of the high air velocity at the outlet section and the cold inlet air, respectively. As an important and desired finding, one can recall the decrease of glass temperature for small value of the duct height b, which is due to the convection enhancement and higher air velocity by the use of narrow air ducts.

One of the main factors for providing the high rate of heat loss and low efficiency of the conventional plane SAHs is the high-temperature absorber plate. To study more about the influence of duct height on this factor, the variations of maximum absorber temperature with air mass flow rate at different values of the parameter b are drawn in Fig. (12). In addition to the decreasing trend of absorber temperature with $\dot{m}$, it is revealed that the designed solar collector can operate with a low absorber temperature under the combined conditions of high air mass flow rate and low value of the duct height. Such that in the case of b=1 cm and mass flow rate of 0.06 kg/s and under the incidence solar radiation of 1000 W/m^2, the absorber temperature is about 50 C.

The thermal efficiency of SAH is one of the main parameters that shows the performance of solar collectors in converting thermal radiation into air enthalpy. To demonstrate the performance of the proposed SAH, the thermal efficiency at different steady conditions is calculated according to the following relation:

$$\eta = \frac{\dot{m} c_p (T_{mout} - T_{in})}{q''_{sun}.A} \tag{9}$$

To examine the effect of air mass flow rate and the sun heat flux on the thermal efficiency, the variations of this parameter with the air mass flow rate at two different solar irradiations are

plotted in Fig. (13). This figure shows the efficiency increase while SAH operates with higher air flow rate, such that the solar irradiation does not have a considerable influence. However, Fig. 13 reveals high thermal efficiencies for the proposed solar collector (0.65 to 0.85) for the range of 0.02 kg/s to 0.06 kg/s air mass flow rate, compared to the conventional plane SAHs. For more study about the performance of circular solar collectors, the effect of parameter b is examined on the variation of η at different air mass flow rates and the results are shown in Fig. 14. As expected, the decrease in the value of duct height leads to performance improvement, especially when SAH operates with a high air mass flow rate.

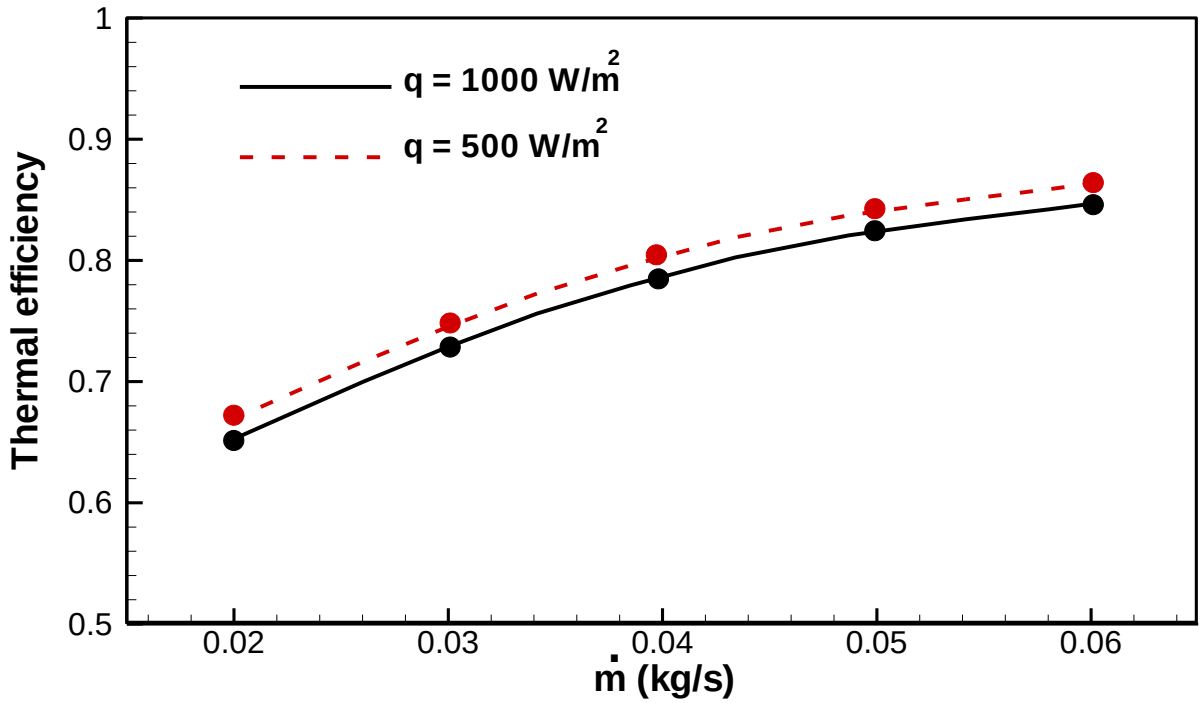

Figure 13 Thermal efficiency variation v.s air mass flow rate, b=1 cm

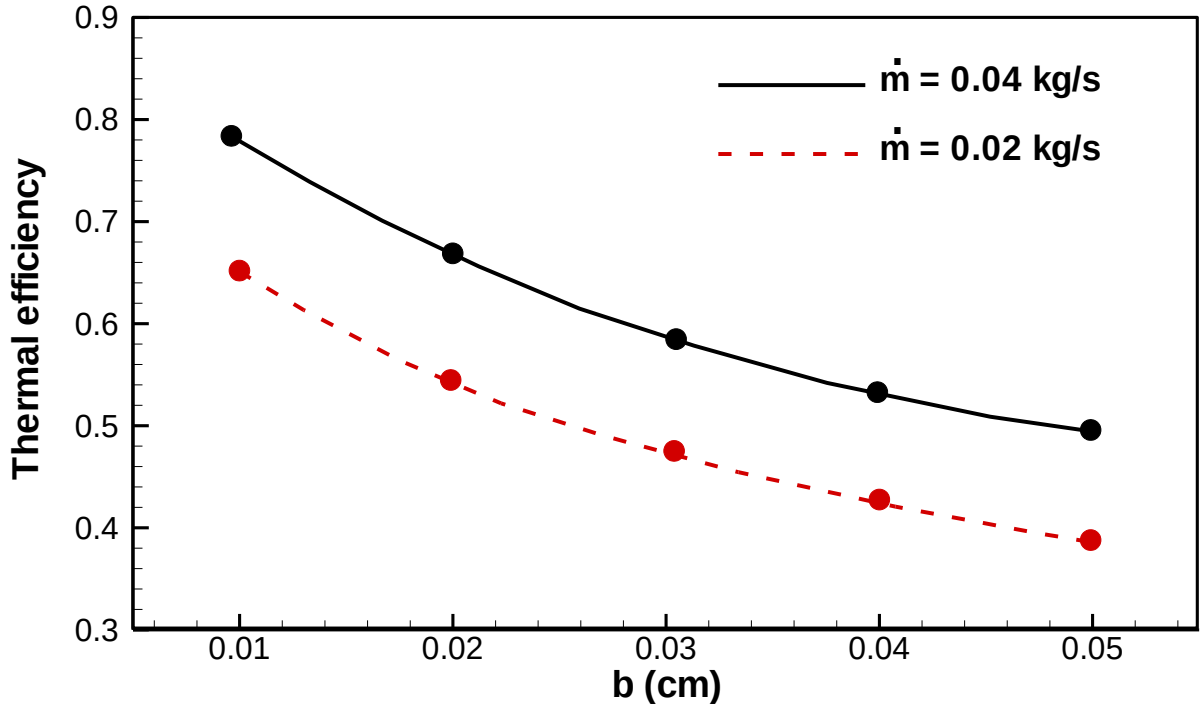

Figure 14 Effect of duct height on thermal efficiency, $q_{sun} = 1000\ W/m^2$

5 Conclusion

One of the best forms of renewable energy is solar energy and the SAHs which usually have simple configurations are useful heat exchangers for converting solar irradiation into air enthalpy. In this article, we performed a CFD-based numerical analysis to examine the benefits of using a new type of circular SAH with radial flow for higher performance. The present numerical analysis involves the solution of flow equations with the finite element scheme by the COMSOL Multi-physics. Numerical findings demonstrate much more thermal efficiency with about 100% improvement compared to conventional solar collectors, especially under the condition of using air ducts with low heights.

References

[1] H. Bhowmik, and R. Amin, "Efficiency Improvement of Flat Plate Solar Collector using Reflector," *Energy Reports*, Vol. 3, pp. 119-123, 2017, doi: https://doi.org/10.1016/j.egyr.2017.08.002.

[2] V. P. Singh, S. Jain, A. Karn, A. Kumar, G. Dwivedi, C. Swaroop Meena, N. Dutt, and A. Ghosh, "Recent Developments and Advancements in Solar Air Heaters: A Detailed Review," *Sustainability*, Vol. 14, No. 19, pp. 12149, 2022, https://doi.org/10.3390/su141912149.

[3] S. K. Samdarshi, and S. C. Mullick, "Analysis of the Top Heat Loss Factor of Flat Plate Solar Collectors with Single and Double Glazing, *International Journal of Energy Research*, Vol. 14, No. 9, pp. 975–990, 1990, https://doi.org/10.1002/er.4440140908.

[4] H. C. Hottel, and B. B. Woertz, "Performance of Flat-plate Solar-heat Collectors," *Journal of Fluids Engineering*, Vol. 64, No. 2, pp. 91–103, 1942, https://doi.org/10.1016/j.ecmx.2022.100247.

[5] T. Alam, and M. H. Kim, "A Critical Review on Artificial Roughness Provided in Rectangular Solar Air Heater Duct," *Renewable and Sustainable Energy Reviews*, Vol. 69, pp. 387–400, 2017, https://doi.org/10.1016/j.rser.2016.11.192.

[6] A. Kumar, R. Kumar, R. Maithani, R. Chauhan, M. Sethi, A. Kumari, S. Kumar and S. Kumar, "Correlation Development for Nusselt Number and Friction Factor of a Multiple Type V-pattern Dimpled Obstacles Solar Air Passage," *Renewable Energy*, Vol. 109, pp. 461–479, 2017, https://doi.org/10.1016/j.renene.2017.03.030.

[7] R. Misra, J. Singh, S. Kumar, S. Faujdar, and M. Agrawal, "Prediction of Behavior of Triangular Solar Air Heater Duct using V-down Rib with Multiple Gaps and Turbulence Promoters as Artificial Roughness: A CFD Analysis, "*International Journal of Heat and Mass Transfer*," Vol. 162, pp. 120376, 2020, https://doi.org/10.1016/j.ijheatmasstransfer.2020.120376.

[8] P. Promvonge, C. Khanoknaiyakarn, S. Kwankaomeng, and C. Thianpong, "Thermal Behavior in Solar Air Heater Channel Fitted with Combined Rib and Delta-winglet," *International Communications in Heat and Mass Transfer*, Vol. 38, pp. 749–756, 2011, https://doi.org/10.1016/j.icheatmasstransfer.2011.03.014.

[9] P. Saravanakumar, D. Somasundaram, and M. Matheswaran, "Exergetic Investigation and Optimization of Arc Shaped Rib Roughened Solar Air Heater Integrated with Fins and Baffles," *Applied Thermal Engineering*, Vol. 175,115316, 2020, https://doi.org/10.1016/j.applthermaleng.2020.115316.

[10] M. Abuska, M. Sevik, and A, Kayapunar, "Experimental Analysis of Solar Air Collector with PCM-honeycomb Combination under the Natural Convection," *Solar Energy Materials and Solar Cells*, Vol. 195, pp. 299–308, 2019, https://doi.org/10.1016/j.solmat.2019.02.040.

[11] A. Tiwari, and A. Kumar, "Solar Air Heater Based on Double-ends Open Evacuated Tube with & without Phase Change Material: An Experimental Investigation," *Journal of Energy Storage*, Vol. 72, Part A, pp. 108265, 2023, https://doi.org/10.1016/j.est.2023.108265.

[12] P. Verma, and L. Varshney, "Parametric Investigation on Thermo-hydraulic Performance of Wire Screen Matrix Packed Solar Air Heater," *Sustainable Energy Technologies and Assessments*, Vol. 10, pp. 40–52, 2015, https://doi.org/10.1016/j.seta.2015.02.002.

[13] A. Kumar, and M.H. Kim, "Solar Air-heating System with Packed-bed Energy-storage Systems," *Renewable and Sustainable Energy Reviews*, Vol. 72, pp. 215–227, 2017, https://doi.org/10.1016/j.rser.2017.01.050.

[14] A. Rasheed, U. Allauddin, H.M. Ali, M. Uzair, P.G. Verdin, and Y.H. Siddiqui, "Heat Transfer and Fluid Flow Characteristics Investigation using Detached Ribs in an Axisymmetric Impinging Jet Flow," *Journal of Thermal Analysis and Calorimetry*, Vol. 147, No. 24, pp. 14517–14537, 2022, https://doi.org/10.1007/s10973-022-11640-w.

[15] U. Allauddin, M.U. Sohail, M. Sohaib, M.A. Siddiqui, M.H.U. Khan, K. Khan, and P.G. Verdin, "Heat Transfer Enhancement Investigation in Jet Impingement System of a Single and Array of Square Jets using Numerical Tools," *Computational Thermal Sciences: An International Journal*, Vol. 15, No. 4, pp. 15-29, 2023, DOI: 10.1615/ComputThermalScien.2023046632.

[16] S. Singh, "Utilising Fractional Porous Interface for High Thermal Performance of Serpentine Wavy Channel Solar Air Heater," *Applied Thermal Engineering*, Vol. 205, pp. 118044, 2022, https://doi.org/10.1016/j.applthermaleng.2022.118044.

[17] M. Moein Addini, and S. A. Gandjalikhan Nassab, "Utilization of Vortex Flow Pattern in the Design of an Efficient Circular Solar Air Heater," *Solar Energy*, Vol. 276, pp. 112683, 2024, https://doi.org/10.1016/j.solener.2024.112683.

[18] S. A. Gandjalikhan Nassab, "Efficient Design of Converged Ducts in Solar Air Heaters for Higher Performance," *Heat Mass Transfer*, Vol. 59, No. 3, pp. 363-375, 2023, https://doi: 10.1007/s00231-022-03228-9.

[19] B. E. Launder, and D. B. Spalding, "The Numerical Computation of Turbulent Flows," *Computer Methods in Applied Mechanics and Engineering*, Vol. 3, No. 2, pp. 269-289, 1974, https://doi.org/10.1016/0045-7825(74)90029-2.

[20] S. Singh, "Performance Evaluation of a Novel Solar Air Heater with Arched Absorber Plate," *Renewable Energy*, Vol. 114, pp. 879–886, 2017, https://doi.org/10.1016/j.renene.2017.07.109.

[21] J. P. Holman, "*Experimental Methods for Engineers*," 6th Edition, McGraw-Hill Series in Mechanical Engineering, McGraw-Hill Inc., Boston, USA, 1994.

[22] F. Chabane, M. Noureddine, and A. Brima, "Experimental Study of Thermal Efficiency of a Solar Air Heater with an Irregularity Element on Absorber Plate," *International Journal of Heat and Technology*, Vol. 36, No. 3, pp. 855-860, 2018, doi.org/10.1016/j.jare.2013.03.001.

Nomenclature

English symbols

A	Area
b	Height of channel (m)
C_p	Specific heat (kJ/kg K)
h	Convection coefficient
k	Thermal conductivity (Wm-1K-1)
p	Pressure (Pa)
q	Heat flux (W/m^2)
R	Radius (m)
Re	Reynolds number
T	Temperature (K)
V	Velocity vector (m/s)
(r, z)	Coordinates (m)

Greek symbols

α_g	Glass absorptivity
ρ_g	Glass reflectivity
τ_g	Glass transmissivity
μ	Fluid Viscosity (Pa.s)
ρ	Fluid density (kg/m)
κ	Turbulence kinetic energy (m^2/s^2)
ε	Surface emissivity
ε	Turbulent dissipation rate (m^2/s^3)

Subscript

abs	Absorber
amb	Ambient
conv	Convection
g	Glass
in	Inlet
ins	Insulation
i, j	Tensor indices
m	Mean
out	Outlet
rad	Radiation
t	Turbulent